

Preparation and properties of 3-aminopropyltriethoxysilane functionalized graphene/polyurethane nanocomposite coatings

Wenshi Ma · Li Wu · Dongqiao Zhang ·
Shuangfeng Wang

Received: 24 April 2013 / Revised: 1 June 2013 / Accepted: 13 June 2013 / Published online: 17 July 2013
© Springer-Verlag Berlin Heidelberg 2013

Abstract Silicone-modified graphene was successfully synthesized by treating graphene oxide with 3-aminopropyltriethoxysilane (AMEO) and then reduced by hydrazine hydrate. Subsequently, the AMEO-functionalized graphene was incorporated into polyurethane (PU) matrix to prepare AMEO-functionalized graphene/PU nanocomposite coatings. The functionalized graphene could disperse homogeneously by means of a covalent connection with PU. AMEO-functionalized graphene (AFG)-reinforced PU nanocomposite coatings showed more excellent mechanical and thermal properties than those of pure PU. A 227 % increase in tensile strength and a 71.7 % improvement of elongation at break were obtained by addition 0.2 wt% of AFG. Meanwhile, thermogravimetric analysis reveals that thermal degradation temperature was enhanced almost 50 °C higher than that of neat PU, and differential scanning calorimetry analysis demonstrates that glass transition temperature decreased by around 9 °C. The thermal conductivity of AFG/PU nanocomposite coatings also increased by 40 % at low AFG loadings of 0.2 wt%.

Keywords Functionalized graphene · Interaction · Polyurethane nanocomposite coatings · Mechanical and thermal properties

Introduction

In the field of material design, the nanocomposites often show all kinds of outstanding performance. Polymer nanocomposites, compared with the pure polymer matrix, possess better mechanical properties and thermodynamic performances [1]. In the past few years, carbon materials, including zero-dimensional fullerene [2], one-dimensional carbon nanotubes [3–5], and three-dimensional diamond [6], have been widely applied in polymer composites. Graphene [7] is a new type of carbon material which was discovered by Konstantin Novoselov and Andre Geim in recent years. It has been attracted a significant interest of scientists because of its remarkable properties, such as ultrahigh specific surface area [8] (2,600 m²/g) and electron mobility [9] (200,000 cm²/(V s)), excellent thermal conductivity [10] (5,000 W/(mK)), and mechanical property [11] (Young's modulus to 1,060 GPa).

However, the liquid-phase production of graphene-based materials is very unstable and severely hampered by the poor solubility of graphene in common organic solvents, which is mainly due to the strong van der Waals attraction between graphene sheets. In order to figure out the problem, the most common method is to modify graphene with micromolecule to achieve a stable dispersion of graphene. Tang [12] and Yoon [13] adopted the pattern of covalent and non-covalent bonds to modify graphene respectively. Then, the nanocomposites of modified graphene/polymer matrix were prepared by a solution blend method and revealed a better performance.

Graphene oxide (GO) is obtained from the oxidization of natural graphite flakes followed by ultrasonic treatment of the suspension. Because of owning large numbers of reactive group, such as hydroxyl, carboxyl, and epoxy groups, GO has been rendered with excellent solubility and dispersibility in organic solvents, which provides the possibility for preparing covalently functionalized oxidation graphene [14]. Meanwhile, modified graphene can be synthesized through a reduction of functionalized oxidation graphene. Based on

W. Ma (✉) · L. Wu · D. Zhang
College of Materials Science and Engineering, South China
University of Technology, Guangzhou 510640, Guangdong, China
e-mail: mcwshma@scut.edu.cn

W. Ma
e-mail: scutlw@163.com

S. Wang
Key Laboratory of Enhanced Heat Transfer and Energy
Conservation of the Ministry of Education, South China University
of Technology, Guangzhou 510640, Guangdong, China

the characteristic of GO, a lot of functional organic substances were grafted to the graphene forming the functionalized graphene, which greatly improved the dispersibility of graphene in the polymer matrix. Stankovich et al. [15] prepared a series of isocyanate-based functionalized graphene by the reaction between GO and isocyanates with small molecular weight, which could be exfoliated into nanoplatelets and kept stable dispersion in many polar solvents, like *N,N*-dimethylformamide (DMF). Under the condition of good dispersion in the solution, functionalized graphene could mix uniformly with polystyrene (PS) to fabricate graphene/PS nanocomposites. Electric percolation threshold equaled to that of the single-walled carbon nanotubes (SWCNT) with the same volume ratio and was two and four times bigger than that of SWCNT/polyimide and SWCNT/polyphenylene ethynylene, respectively. Ramanathan et al. [16] synthesized functionalized graphene/polymethyl methacrylate (PMMA) nanocomposites. The glass transition temperature (T_g) of nanocomposite had been improved nearly 30 °C in comparison with the neat PMMA, and the elastic modulus and hardness were increased by 30 and 5 %, respectively.

In recent years, some researchers have applied functionalized graphene into polyurethane materials. Kim et al. [17] reported a kind of thermoplastic polyurethane elastomer, which possessed excellent air impermeability and electrical properties by addition of functionalized graphene. Lee et al. [18] researched that functionalized graphene nanosheets could be incorporated to water-borne polyurethane (WPU) in situ polymerization method. The transmission electron microscopy (TEM) images show that pristine nanosize functionalized graphene nanosheets could be finely dispersed in WPU matrix, which gives rise to the efficient improvement of the conductivity. The modulus and crystallization of the soft segment of WPU were evidently enhanced. However, thermal degradation was accelerated.

As is well-known, the polyurethane coating is applied more and more widely, but few studies have focused on the thermal conductivity coatings [19–22]. In this paper, the functionalized graphene with reactive hydrogen was synthesized and could react with isocyanate group of PU to form graphene/PU nanocomposite coatings (the synthetic approach and structure of graphene/PU can be seen in Fig. 1) which provided outstanding thermal and mechanical properties so that it is a potential candidate to be used as thermal conductivity coatings.

Experimental

Raw materials

Toluene diisocyanate (TDI) was obtained from Japan; polycaprolactone polyol (PCL-1000) was dehydrated about

2–3 h at 120–130 °C under vacuum with molecular weight of about 1,000 g/mol and hydroxyl value of around 112 mg KOH/g from Shenzhen Guanghua Weiye Co., Ltd. The 4A molecular sieve with globular Φ 3–5 mm was purchased from Shanghai Runhai Rapid Chemical Reagent Co., Ltd. The graphite powder had a particle size of \sim 70 μ m with a purity of 99.9 % and a density of 2.25 g/cm³. The reagents and solvents were used as follows: anhydrous ethanol (CH₃CH₂OH; Tianjin Fuyu Chemical Co., Ltd.), dimethylbenzene (Jiangsu Qiangsheng Chemical Co., Ltd.), DMF (Jiangsu Qiangsheng Chemical Co., Ltd.), triethylamine (Tianjin Bodi Chemical Co., Ltd.), hydrazine hydrate (Tianjin Fuchen Chemical Reagent Factory), dibutylamine (Shanghai Ethyl Chemical Co., Ltd.), and trimethylolpropane (TMP; Shanghai Ethyl Chemical Co., Ltd.). The 3-aminopropyltriethoxysilane (AMEO) was obtained from Aldrich. All solvents were used after further dehydration.

Synthesis of AMEO-functionalized graphene

The synthesis process of AMEO-functionalized graphene was as follows: in a typical step, GO was prepared from a modified method of Hummers [23]; 100 mg of GO was loaded into a 250-ml round-bottom flask in 150 ml of alcohol–water solution (2:1 v/v) by ultrasonication dispersion; and 0.10 ml of triethylamine and 1.00 g of AMEO were added into the flask equipped with stirring for 24 h in room temperature. The slurry reaction mixture was filtered and washed with additional anhydrous ethanol in order to remove residual AMEO and then washed with deionized water to achieve neutral. Subsequently, the product without drying was added into 100 ml of deionized water before another ultrasonic dispersion; 1.00 g and above of hydrazine hydrate mixture were transferred to a round-bottom flask and stirred for 24 h at 90 °C under a nitrogen condition. Residual hydrazine hydrate and other materials were removed by centrifugal sedimentation and ultrasonic dispersion (using ethanol and water) cycles, which processes were repeated at several times. The final product was dried in a vacuum and then preserved.

Preparation of PU coatings

The mixture with 6.96 g of TDI and a moderate amount of dimethylbenzene in a four-neck flask equipped with agitator and thermometer under a nitrogen condition was heated in water bath. To keep at NCO/OH molar ratio of 2:1, 10.00 g of PCL-1000 and 0.89 g of TMP which was dissolved in xylene and fabricated mixed solution. When the temperature increased to 50 °C, the mixed solution was slowly poured into the above four-neck flask by means of constant pressure funnel during 1 h. The hybrid solution was heated to 70 °C, and the reaction continued until the content of NCO arrived at the theoretical value.

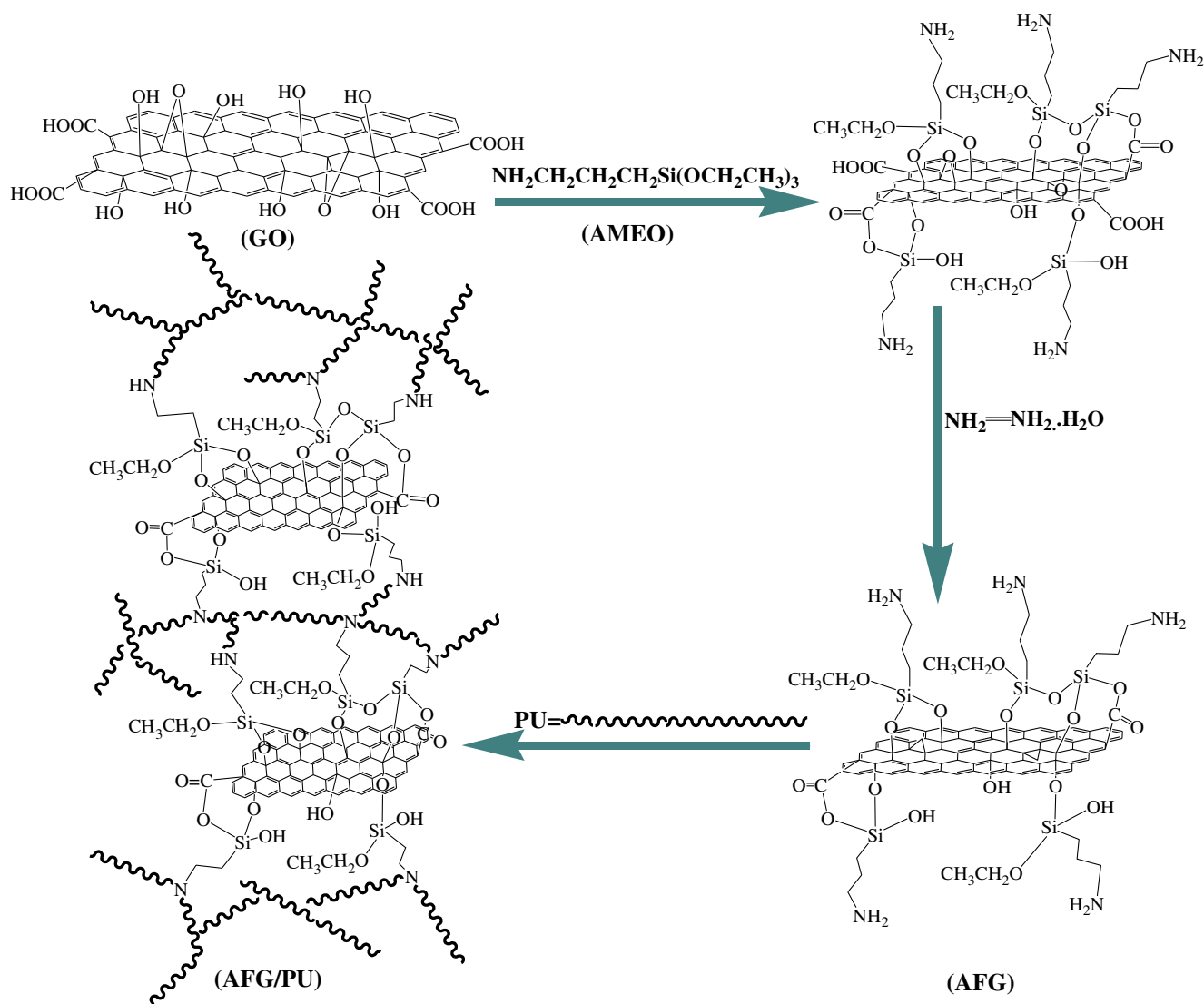


Fig. 1 Schematic illustration of the fabrication of AFG/PU nanocomposite coatings

Fabrication of AMEO-functionalized graphene/PU nanocomposite coatings

The formulation of AMEO-functionalized graphene (AFG)/PU nanocomposite coatings is explicitly shown in Table 1; 5 mg of the synthetic AFG was uniformly dispersed in DMF solvents under ultrasonication. Then, 25.00 g of fabricated PU was added to the above well-dispersed AFG suspension at room temperature and stirred for 1 h in a flask. Afterwards, the mixed solution of AFG/PU was casted into a polytetrafluoroethylene (PTFE) mold and was dried at room temperature for 3 days. The wetting coating was heated at 70 °C for 12 h. AFG/PU nanocomposite coating with different loadings was prepared with similar process. Finally, AFG/PU coatings were peeled off the PTFE carefully and used for the tests of thermostability and mechanical performance.

Characterization and instruments

Fourier transform infrared spectroscope (FT-IR) were recorded using the American Analect RFX-65 Fourier transform infrared spectrometer in KBr pellets and scanned from 4,000 to 400 cm^{-1} with a resolution ratio (4 cm^{-1}). X-ray diffraction (XRD) was

Table 1 Formulations of AFG/PU nanocomposite coatings

Sample	AFG/mg	PU (solid content 40 %)/g	AFG (wt%)
PU	0	25.00	0
AFG/PU-1	5	25.00	0.05
AFG/PU-2	10	25.00	0.1
AFG/PU-3	20	25.00	0.2

carried out in Germany D8 ADVANCE diffractometer equipped with Cu K α radiation ($\lambda=0.154$ nm, 40 kV, 40 mA) as the X-ray source. The sample was tested with scanning from 5° to 60° , 0.02° of scanning step length, and 0.1 s/length of scanning speed. X-ray photoelectron spectroscopy (XPS) measurements were performed using a monochromic Al K α (1,486.6 eV) source at 15 kV and 10 mA on the Kratos Axis Ultra DLD spectrometer. Thermogravimetric analysis, using the Germany NETZSCH TG 209 types of differential thermogravimetric analyzer, was used to measure the thermal stability of the materials at a heating rate of $10^\circ\text{C}/\text{min}$ in a N_2 atmosphere from 0 to 700°C . SPI3800-APA-400 atomic force microscopy (AFM) observation, made in Japan Seiko Instruments Company, was performed in a tapping mode using the rectangular Si 3N_4 probe. Scanning electron microscopy (SEM) was performed on a field emission scanning electron microscope (JEOL JSM-6700F) and used to explore morphology properties. Differential scanning calorimetry (DSC) analysis meter which was made in Germany NETZSCH Company was performed from -80 to 100°C at a heating rate of $20^\circ\text{C}/\text{min}$, with a nitrogen condition at a rate of 50 ml/min. Thermal conductivity of composites was measured by the Thermal Constant Analyzer (TPS 2500; Hot Disk Co., Sweden) at room temperature. The UT-2080 electronic universal material testing machine was used to measure the tensile strength and elongation at break following the GB/T 582–1988, at the rate of extension of 100 mm/min.

Results and discussion

Structure characterization of GO and AFG

The FT-IR results of GO and AFG are shown in Fig. 2. From the spectrum of GO, it can be found that the absorption peak at around $3,432$ and $1,702$ cm^{-1} is respectively ascribed to the stretching vibration of hydroxyl and carboxyl groups on the GO surface. The adsorption peak at $1,626$ and $1,056$ cm^{-1} is due to the stretching vibration of benzene ring

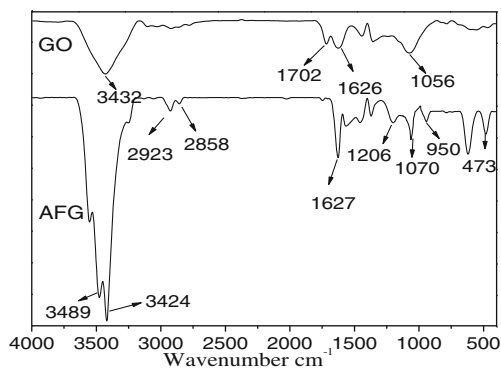


Fig. 2 FT-IR spectra of GO and AFG

structure and $-\text{C}-\text{O}-$ in epoxide groups, respectively. After treatment with AMEO and triethylamine, the sharp characteristic peaks at $3,489$ and $3,424$ cm^{-1} appeared, which are attributed to the characteristic absorption of primary amine ($-\text{NH}_2$) from AMEO. The doublet at $2,923$ and $2,858$ cm^{-1} corresponding to symmetric and asymmetric vibrations of the $-\text{CH}_2-$ group are assigned to the alkyl chains for AMEO of AFG. The stretching vibration of benzene ring structure from AFG at $1,627$ cm^{-1} is obviously stronger than that of GO, which illustrates that functionalized GO recovered to the benzene ring structure by the reduction with hydrazine hydrate. In addition, the absorption bonds of AFG at $1,070$ cm^{-1} could be represented for stretching vibration absorption peak of $\text{Si}-\text{O}-\text{Si}$ [24–27], which can be interpreted because of the mutual hydrolytic condensation of AMEO in the process of functionalized graphene. The new absorption peaks at 950 and 473 cm^{-1} are from stretching vibration and deformation vibration of $\text{Si}-\text{O}-\text{Ph}$ [28, 29]. These characteristic absorption peaks indicated that the AMEO was successfully attached to the GO surface, and the most residual oxygen-containing groups, which did not react with the AMEO molecules, were removed at the same time.

XRD analysis was employed to further illustrate the surface structure of GO and AFG. Figure 3 shows the XRD pattern of starting graphite, GO, and AFG. For the graphite, a very sharp peak at $2\theta=26.44^\circ$ can be accounted for the (002) characteristic diffraction peak of graphite and figured out 0.34 nm of the interlayer spacing, which is in accordance with the thickness of single graphene [7]. For the GO sample, the diffraction peak shifted to $2\theta=10.71^\circ$ corresponding to an interlayer spacing of 0.83 nm, which is ascribed to the (001) diffraction peak of GO [30]. The phenomenon is due a lot to the generation of oxygen-containing functional groups after oxidization, which made interlayers spacing of GO bigger. In the desiccative process, GO nanosheets were easy to agglomerate and accumulate orderly because of the formation of hydrogen

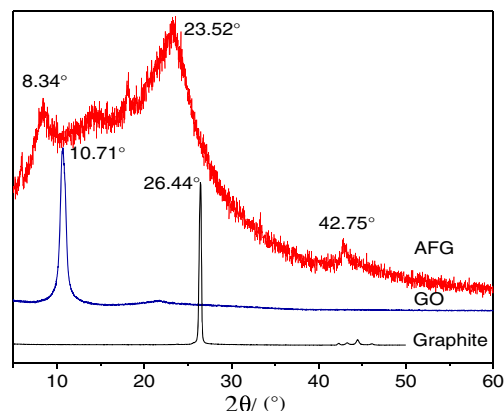


Fig. 3 The XRD spectra of graphite, GO, and AFG

bond among the nanosheets. So a sharp peak appeared in the spectrum of GO. The XRD spectrum of AFG shows three obvious peaks. The peak at $2\theta=8.34^\circ$, corresponding to interlayers spacing of 1.06 nm, is expected from the grafted AMEO regions on the graphene sheets. The interlayers spacing increase from GO of 0.83 nm to AFG of 1.06 nm was due to the introduction of AMEO molecules. The other two widish peaks at $2\theta=23.52^\circ$ and $2\theta=42.75^\circ$ are expressed by the (002) and (100) diffraction peaks of graphene [30]. Comparing the peak at $2\theta=23.52^\circ$ of AFG with the peak at $2\theta=26.44^\circ$ of graphite, the interlayers spacing of AFG is still larger than that of the graphite for the introduction of AMEO, even after efficient reduction. These results indicate that oxygen-containing functional groups were removed from functionalized GO through the reduction of hydrazine hydrate and restored the crystal structure of graphite. However, there is a reduction in both crystal shape and size and increment in crystal imperfection, resulting in an increasing disorder and broadening of the diffraction peak.

To provide further the evidence of the AMEO which was introduced in the surface of AFG, the C1s spectra of both GO (Fig. 4c) and AFG (Fig. 4d) were provided. As shown in Fig. 4c, the C1s of GO could be deconvoluted into four peaks corresponding to carbon atoms in different functional groups: C=C/C-C (non-oxygenated carbon, 284.6 eV), C-O-C (epoxy, 286.6 eV), C=O (carbonyl, 288.2 eV), and C-OH

(hydroxyl, 285.6 eV). After functionalization with AMEO (Fig. 4b), the peaks corresponding to oxygen weakened significantly (Fig. 4a), and new peaks to C-Si (283.7 eV) and C-O-Si (285.4 eV) appeared, implying that AFG was prepared by the reaction between GO sheets and AMEO.

Morphological properties

Morphology observation is the most direct way to estimate the attachment effect of nanoparticles on GO sheets. In order to measure the thickness of GO and AFG, the tapping mode AFM images of GO and AFG (both of dispersed in DMF) are shown in Fig. 5. It can be seen that GO and AFG nanoplatelets dispersed in DMF so well and did not aggregate. The average thickness of GO and AFG nanosheets is around 0.755 and 1.104 nm, respectively, which is close to the height of single-layer GO and AFG (0.83 and 1.06 nm) measured by XRD, indicating that complete exfoliation between nanosheets and single layer occurred. The AFG nanoplatelets were thicker than those of GO, which is attributed to functionalized AMEO chains grafting on the graphene nanosheets and is consistent with Yang's finding [25].

The theoretical structure representation of pure PU and AFG/PU composite can be simulated in Fig. 6a, b. The dispersion level of the AFG in PU matrix and the interfacial interaction between the AFG and PU matrix play a key role in

Fig. 4 XPS scanning spectra of GO (a), AFG (b) and C1s of GO (c), and AFG (d)

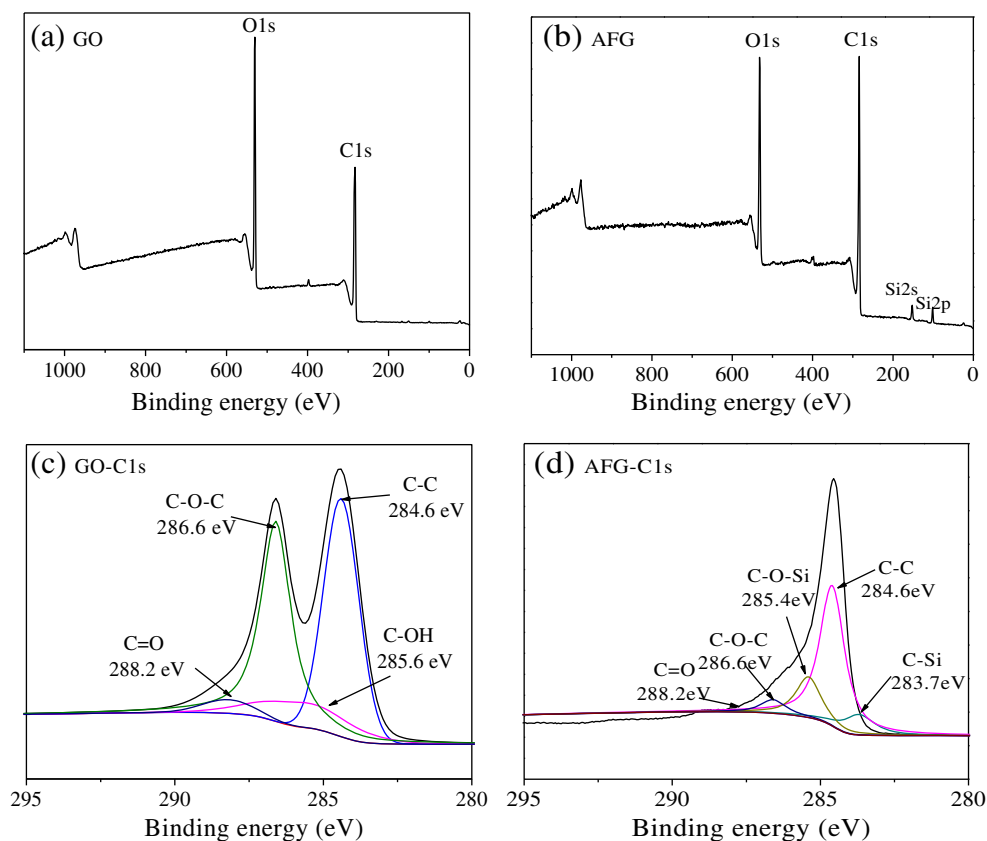
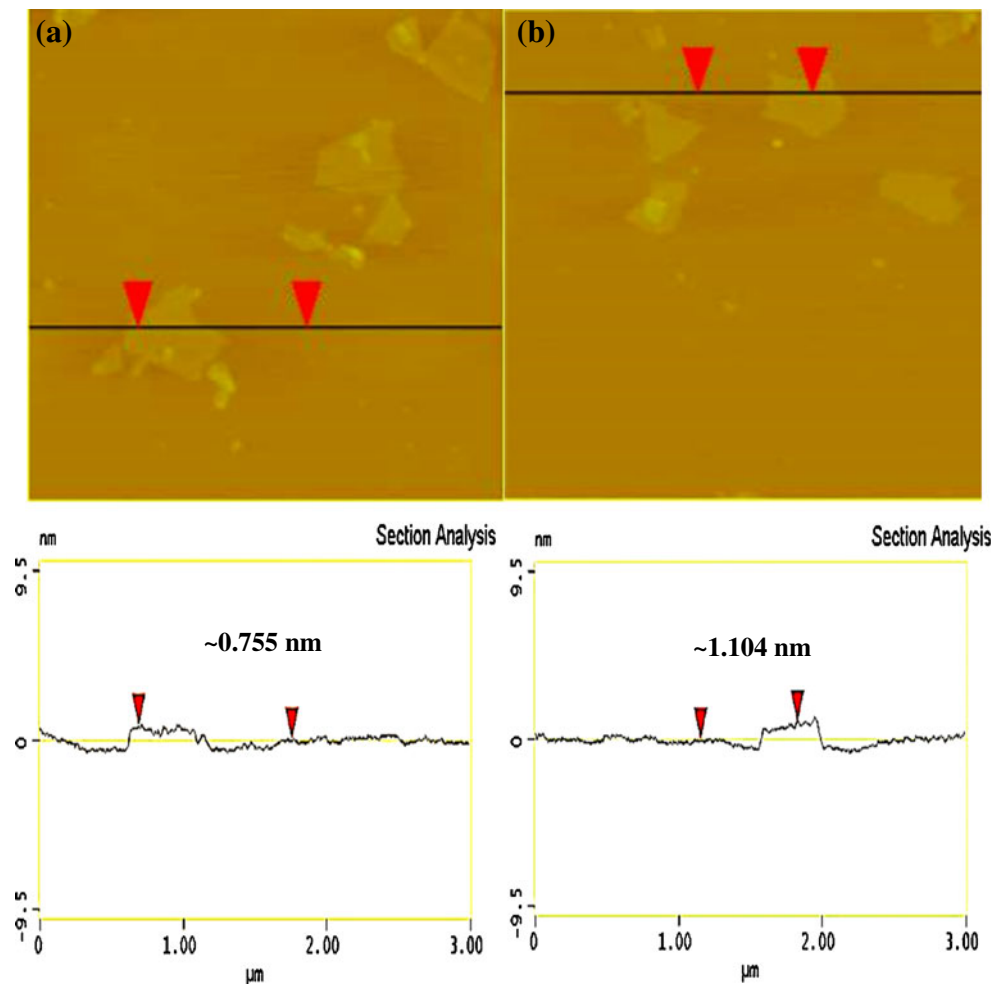


Fig. 5 AFM images of GO (a) and AFG (b)



the improvement in the tensile strength and thermodynamic property of AFG/PU nanocomposite coatings. The different magnification SEM images of AFG/PU nanocomposite coating (0.2 wt% of AFG) as shown in Fig. 6c, d reveal that AFG nanoplatelets dispersed well in PU matrix. The fuzzy interface between AFG and PU matrixes indicates a strong chemical bond ($-\text{NH}-\text{CO}-\text{NH}-$) formed for the reaction between $-\text{NH}_2$ on the AFG and $-\text{NCO}$ groups on the end of PU chains.

Mechanical properties

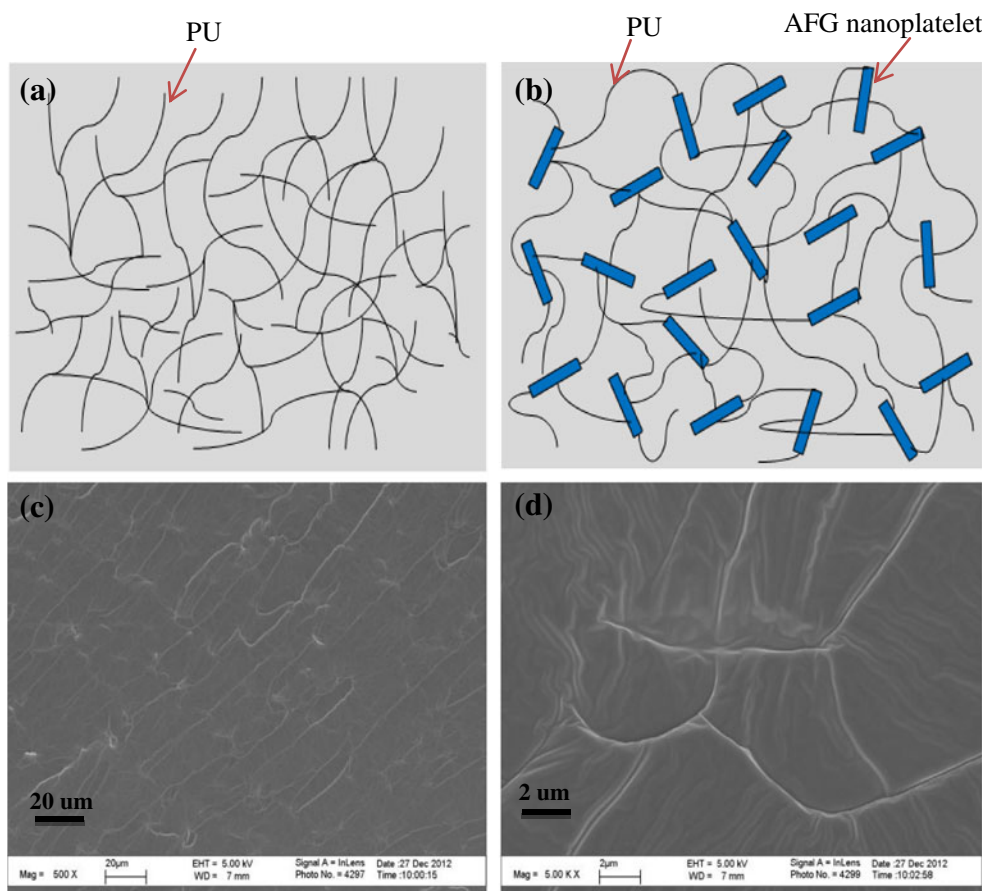
Tensile strength and elongation at break of AFG/PU nanocomposite coatings with different AFG contents are shown in Fig. 7. The PU reinforced by addition of AFG nanoplatelets showed a better tensile property than that of neat PU. At the same time, it was also found that the tensile strength and elongation at break increased with increasing AFG contents. When compared with pure PU, the tensile strength and elongation at break of AFG/PU nanocomposite coatings increased by 227 and 71.7 %, respectively, at addition of AFG of 0.2 wt%. The result implies that the movement of chain segments in PU matrix was limited due to the strong interfacial interaction between AFG nanoplatelets and

PU, which is responsible for the increment of tensile strength. PU chain could graft on the surface of AFG by reaction between aminos of AFG surface and isocyanate groups at the end of PU, which was a similar role to carbon black reinforcing. However, it is uncommon that the changing trend of elongation at break was consistent with tensile strength. It could be explained that biuret structure formed on the AFG nanoplatelets surface for AFG/PU nanocomposite coatings, while biuret structure of neat PU was mainly produced among PU chain segments, which led to higher toughness of AFG/PU nanocomposite coatings.

Thermal properties

The TG graphs for neat PU and AFG/PU nanocomposite coatings under nitrogen atmosphere are shown in Fig. 8. A sharp decrease in weight loss between 250 to 450 °C for both the neat PU and AFG/PU nanocomposite coatings could be ascribed to decomposition of polyurethane resin. The weight loss below 250 °C is attributed to the volatilization of a small amount of organic solvents in PU coatings. For the TG curve of AFG/PU, it can be seen that the thermostability of AFG/PU nanocomposite coatings is obviously better than

Fig. 6 Structural representation of PU (a) and AFG/PU (b) and different magnification SEM images of AFG/PU nanocomposite coatings (c, d)



that of neat PU for addition of AFG in PU matrix. The temperature which is stemmed from point of intersection between the tangent line of decreasing step and base line is used to represent the thermal stability of the materials. It was found that the thermal stability temperature of neat PU was 274.2 °C. After adding AFG of 0.05 wt%, the PU

nanocomposite coatings are approximately 33 °C higher than those of neat PU, which means that the thermal stability of the nanocomposite coating was remarkably enhanced. With the increase of the content of AFG, thermal stability

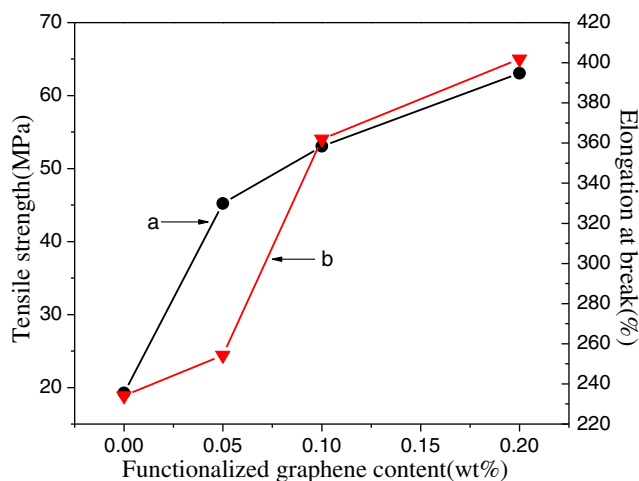


Fig. 7 Tensile strength (a) and elongation at break (b) related to functionalized graphene content

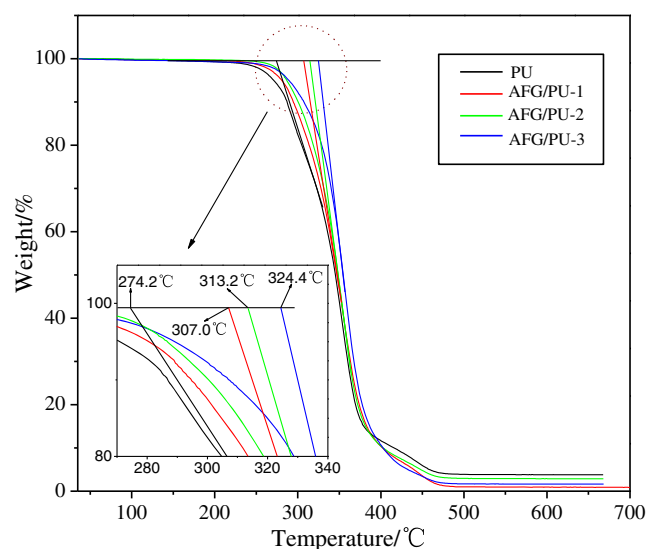


Fig. 8 The TG curve graph of PU and AFG/PU nanocomposite coatings

temperature of AFG/PU nanocomposite coatings continuously improved and attained 324.4 °C at 0.2 wt% of AFG. The reason of the increase in the thermal stability temperature can be that additional AFG has played a key role in delaying the permeation of oxygen and the escape of volatile degradation products, namely, the “tortuous path” effect of graphene sheets [31]. In addition, low load quantity of graphene sheets can improve the performance of the composite materials because of the ultrahigh specific surface area [7]. Ramanathan et al. [16] had reported that the fraction requirement of graphene sheets in the composites was around 0.05 wt% for rheological penetration performance, which is consistent with our experimental results.

The effect of AFG content in nanocomposite coatings on the T_g was studied by DSC. Figure 9 shows the DSC curves of PU, AFG/PU-1, AFG/PU-2, and AFG/PU-3 nanocomposite coatings. From the graph, it can be seen that the T_g of pure PU is approximately -20.2 °C, while the T_g of prepared AFG/PU nanocomposite coatings is approximately -23.5 , -25.7 , and -29.1 °C for AFG/PU-1, AFG/PU-2, and AFG/PU-3, respectively. It reflects that the T_g of PU gradually decreased with the increase of the content of AFG. In addition, the curve of neat PU did not show an obvious inflection point, while the curves of AFG/PU nanocomposite coatings demonstrated the echelonments and obvious inflection points. This implied that the movement of chain segments of neat PU was a stronger obstacle than that of AFG/PU nanocomposite coatings in the glass transition process, which was caused by forming different bonds in the curing process. After curing at room temperature, the urea bond of neat PU could continue reacting with excess isocyanate groups to produce a lot of biuret structures in high temperature, which produced intense interaction between chain segments of neat PU and made segments difficult to move. However, the $-NH_2$ groups of AFG nanoplatelets were prone to react with isocyanate groups of PU in room temperature, which gave rise to a lesser biuret structure in the

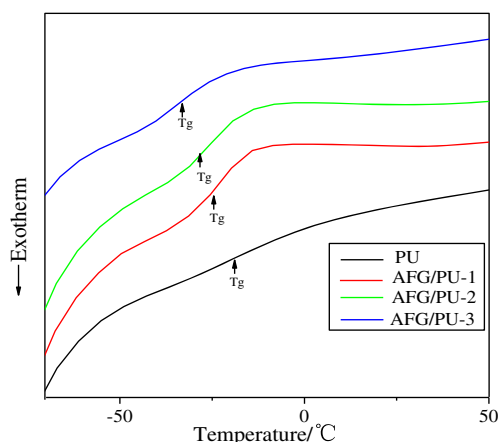


Fig. 9 The DSC curves of neat PU, AFG/PU-1, AFG/PU-2, and AFG/PU-3 nanocomposite coatings

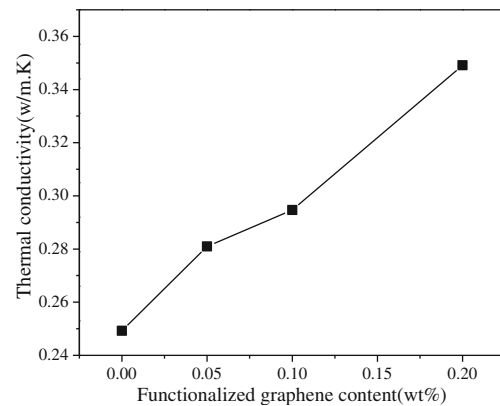


Fig. 10 Thermal conductivity of neat PU and AFG/PU nanocomposite coatings

high temperature curing. Meanwhile, introducing AFG nanoplatelets into PU increased the distance between PU chains segments so that interaction between chains segments of nanocomposite coatings turned weak, resulting in a better flexibility.

The thermal conductivities of neat PU and its nanocomposite coatings filled with AFG are shown in Fig. 10. As expected, thermal conductivity is considerably enhanced by the presence of AFG. It can be seen that with 0.05, 0.1, and 0.2 wt% AFG, the thermal conductivities of AFG/PU nanocomposite coatings increase by 13, 18, and 40 % to 0.2810, 0.2947, and 0.3491 W/mK from 0.2492 of neat PU, respectively. It is well-known that phonon propagation affects directly the thermal conductivity of materials. So this increase can be attributed to the high thermal conductivity of the network of AFG that provides a path of lower resistance for phonons to spread. Also, the high aspect ratio and large interfacial contact area of AFG as well as strong interface between graphene and polymer may help to increase the thermal transport capacity of AFG/PU nanocomposite coatings. With a view to the very high theoretical thermal conductivity of graphene [10] (5,000 W/mK), one might expect a more dramatic improvement in thermal conductivity of the composite with the addition of graphene fillers. However, it has been reported that since the dominant heat transfer mechanism is due to the lattice vibrations or phonons. Poor phonon coupling cause thermal resistance in the vibrational modes at the polymer–filler and filler–filler interfaces, which decreases the overall thermal conductivity of the material [32–34].

Conclusions

In this study, we have successfully prepared the AFG/polyurethane nanocomposite coatings by a solution blend method. AFG was synthesized by treating GO with AMEO and hydrazine hydrate reduction. The results from FT-IR and XPS

confirmed the structure of AFG. AFM analysis demonstrates that the thickness of exfoliated AFG was around 1.104 nm. SEM images show that AFG was dispersed well in PU matrix due to the good interfacial interaction between AFG and PU. The prepared AFG/PU nanocomposite coatings presented a great reinforced effect on the mechanical and thermal properties, which were mostly attributed to the strong interfacial interaction between the AFG and PU. The TG measurement shows that the thermal stability temperature is approximately 50 °C higher than that of the neat PU at the AFG loadings of 0.2 wt%. Meanwhile, glass transition temperature decreases by about 9 °C. Additionally, the tensile strength and elongation at break of the AFG/PU nanocomposite coatings increase by 227 and 71.7 %, respectively. The thermal conductivities of PU matrix are also significantly boosted by adding AFG. These results indicate that adding functionalized graphene to polymer matrix will provide a promising approach to fabricate polymeric nanocomposite coatings with excellent performances.

Acknowledgments We acknowledge the financial support from both the National Natural Science Foundation of China (51072059) and Guangdong Science and Technology Project (2011A081301018).

References

- Potts JR, Dreyer DR, Bielawski CW, Ruoff RS (2011) Graphene-base polymer nanocomposites. *Polymer* 52:5–25
- Naffakh M, Diez-Pascual AM, Gomez-Fatou MA (2011) New hybrid nanocomposites containing carbon nanotubes, inorganic fullerene-like WS₂ nanoparticles and poly(ether ether ketone) (PEEK). *J Mater Chem* 21:7425–7433
- Arai S, Sato T, Endo M (2011) Fabrication of various electroless Ni–P alloy/multiwalled carbon nanotube composite films on an acrylonitrile butadiene styrene resin. *Surf Coat Tech* 205:3175–3181
- Reddy KR, Jeong HM, Lee Y, Raghu AV (2010) Synthesis of MWCNTs-core/thiophene polymer-sheath composite nanoscables by a cationic surfactant-assisted chemical oxidative polymerization and their structural properties. *Polym Chem* 48:1477–1484
- Keshri AK, Patel R, Agarwal A (2010) Comprehensive process maps to synthesize high density plasma sprayed aluminum oxide composite coatings with varying carbon nanotube content. *Surf Coat Tech* 205:690–702
- Abyzov AM, Kidalov SV, Shakhov FM (2012) High thermal conductivity composite of diamond particles with tungsten coating in a copper matrix for heat sink application. *Appl Therm Eng* 48:72–80
- Novoselov KS, Geim AK, Morozov SV et al (2004) Electric field effect in atomically thin carbon films. *Science* 306:666–669
- Chae HK, Siberio-Perez DY, Kim J et al (2004) A route to high surface area, porosity and inclusion of large molecules in crystals. *Nature* 427:523–527
- Lee C, Wei X, Kysar JW et al (2008) Measurement of the elastic properties and intrinsic strength of monolayer graphene. *Science* 321:385–388
- Balandin AA, Ghosh S, Bao W et al (2008) Superior thermal conductivity of single-layer graphene. *Nano Lett* 8:902–907
- Bolotin KI, Sikes KJ, Jiang Z et al (2008) Ultrahigh electron mobility in suspended graphene. *Solid State Commun* 146:351–355
- Tang ZH, Lei YD, Guo BC et al (2012) The use of rhodamine B-decorated graphene as a reinforcement in polyvinyl alcohol composites. *Polymer* 53:673–680
- Yoon IS (2011) Role of poly(*N*-vinyl-2-pyrrolidone) as stabilizer for dispersion of graphene via hydrophobic interaction. *J Mater Sci* 46:1316–1321
- Jaemyung K, Laura JC et al (2012) Two-dimensional soft material: new faces of graphene oxide. *Acc Chem Res* 45:1356–1364
- Stankovich S, Piner RD, Nguyen ST et al (2006) Synthesis and exfoliation of isocyanate-treated graphene oxide nanoplatelets. *Carbon* 44:3342–3347
- Ramanathan T, Abdala AA, Stankovich S et al (2008) Functionalized graphene sheets for polymer nanocomposites. *Nat Nanotechnol* 3:327–331
- Kim H, Miura Y, Macosko CW (2010) Graphene/polyurethane nanocomposites for improved gas barrier and electrical conductivity. *Chem Mater* 22:3441–3450
- Lee YR, Raghu AV, Jeong HM, Kim BK (2009) Properties of waterborne polyurethane/functionalized graphene sheet nanocomposites prepared by an in situ method. *Macromol Chem Phys* 210:1247–1254
- Leivo EM, Keltberg TH, Kotari MJ (2001) Structure and thermal conductivity of flame sprayed polyamide 11 coatings filled with AlN, Al₂O₃ and BN ceramics. *ASM Int Mater Park* 204:327–330
- Lu X, XU G, Hofstra PG (1998) Moisture absorption, dielectric relaxation, and thermal conductivity studies of polymer composites. *J Polym Sci* 36:2259–2265
- Choy CL (1977) Thermal conductivity of polymer. *Polymer* 18:984–1004
- Zhou WY, Qi SH et al (2007) High temperature and insulating heat conductive coating. *Acta Materiae Compositae Sinica* 24:28–32
- Hummers W, Offeman R (1958) Preparation of graphitic oxide. *J Am Chem Soc* 80:1339–1339
- Yuen SM, Ma CCM, Chiang CL (2008) Silane-grafted MWCNT/polyimide composites preparation, morphological and electrical properties. *Compos Sci Technol* 68:2842–2848
- Yang H, Li F, Shan C, Han D, Zhang Q, Niu L, Ivaska A (2009) Covalent functionalization of chemically converted graphene sheets via silane and its reinforcement. *J Mater Chem* 19:4632–4638
- Hemraj-Benny T, Wong SS (2006) Silylation of single-walled carbon nanotubes. *Chem Mater* 18:4827–4839
- Hou SF, Su SJ, Kasner ML, Shah P, Patel K, Madarang CJ (2010) Formation of highly stable dispersions of silane-functionalized reduced graphene oxide. *Chem Phys Lett* 501:68–74
- Pinto PR, Menders LC, Dias ML, Azuma C (2006) Synthesis of acrylic-modified sol–gel silica. *Colloid Polym Sci* 284:529–535
- Prassas M, Phalippou JL, Mench L, Zarzycki J (1982) Preparation of $x\text{Na}_2\text{O}-(1-x)\text{SiO}_2$ gels for the gel-glass process: I. Atmospheric effect on the structural evolution of the gels. *J Non-Cryst Solids* 48:79–95
- Stankovich S, Dikin DA, Piner RD, Kohlhaas KA, Kleinhammers A, Jia Y, Wu Y, Nguyen ST, Ruoff RS (2007) Synthesis of graphene-based nanosheets via chemical reduction of exfoliated graphite oxide. *Carbon* 45:1558–1565
- McLauchlin AR, Thomas NL (2009) Preparation and thermal characterisation of poly(lactic acid) nanocomposites prepared from organoclay based on an amphoteric surfactant. *Polym Degrad Stab* 94:868–872
- Zhong H, Lukes JR (2006) Interfacial thermal resistance between carbon nanotubes: molecular dynamics simulations and analytical thermal modeling. *Phys Rev B: Condens Matter* 74:1–10
- Huxtable S, Cahill D, Shenogin S, Xue L, Ozisik R, Barone P, Usrey M, Strano M, Siddons G, Shim M, Keblinski P (2003) Interfacial heat flow in carbon nanotube suspensions. *Nat Mater* 2:731–734
- Shenogin S, Liping X, Ozisik R, Keblinski P (2004) Role of thermal boundary resistance on the heat flow in carbon-nanotube composites. *J Appl Phys* 95:8136–8144